THE OPTICAL LAYOUT OF THE HEGRA CHERENKOV TELESCOPES

A. AKHPERJANIAN, R. KANKANIAN and V. SAHAKIAN
Yerevan Physics Institute, Yerevan, Armenia

A. HEUSLER, C.-A. WIEDNER and H. WIRTH
Max-Planck-Institut für Kernphysik, Heidelberg, Germany

(Received 22 January 1997; accepted in revised form 22 May, 1997)

Abstract. The raytracing technique was used to derive a suitable design for the HEGRA system of Cherenkov telescopes, which is at present commissioned at La Palma. The reflectors with a diameter of $\sim$ 3.9 m consist of 30 spherical mirrors with focal lengths in the range of 4.88 – 4.94 m. It is shown that 93% of the photons from the Cherenkov light emitted by an extended air shower are contained in the camera pixels, 0.25° in diameter, for the full field of view of $\vartheta = \pm 2.5°$. The optical performance of the HEGRA design is compared to other layouts.

Keywords: Optical layout, Cherenkov telescope, Very high energy gamma ray astronomy

1. Introduction

The detection of γ-radiation from astrophysical sources at energies $E_\gamma < 30$ GeV with satellites – especially the CGRO mission with its EGRET detector has rather unexpectedly shown that more than 100 quite different galactic and extragalactic objects, e.g. SNR's, pulsars, AGNs etc. have strong γ-emissivity [1]. At very high γ-energies (VHE), i.e. in the TeV-regime (1 TeV = 10^{12} eV), the fluxes are small and large terrestrial detectors with collection areas of $>10^8$ cm^2 are superior to satellite devices with a few 10^2 cm^2. Since the earth's atmosphere is opaque for VHE γ-radiation, the Cherenkov light emission from relativistic charged particles must be detected, where the latter are due to the interaction of the primary γ-quanta with atmospheric oxygen and nitrogen nuclei leading to a shower. Due to the shower development and its lateral distribution the detection area for Cherenkov light is $\geq 10^5$ times larger than that of satellite detectors.

With the Imaging Air Cherenkov Technique (IACT) flashes of light with a duration of 3-5 ns are collected with large reflectors and registered by a camera with up to several 100 detector pixels. Showers are also released by protons and heavier nuclei of the isotropic cosmic radiation. This flux is at least 10^3 times higher than the expected γ-fluxes and must be efficiently discriminated and suppressed, which is accomplished by an analysis of the Cherenkov light distribution obtained with the camera of the telescope. Indeed the only so far unambigiously established sources of γ-radiation in the VHE regime have been discovered employing the IACT [2].

Experimental Astronomy **8:** 135–152, 1998.

The HEGRA (**H**igh **E**nergy **G**amma **R**ay **A**stronomy) collaboration decided to add a system of Cherenkov telescopes [3] to the existing cosmic ray detectors on the Canarian island of La Palma (17°45′ W, 28°55′ N). There, due to superb seeing conditions also several optical telescopes are operated at the site of the Roque de los Muchachos (at 2200 m asl) hosted by the Instituto Astrofisico de Canarias (IAC). In 1992 the HEGRA collaboration commissioned a prototype telescope described in ref. [4]. Since 1993 a larger telescope with a reflector of $\sim$ 3.9 m in diameter is operating and in 1995 the second telescope of the array was commissioned. Four additional telescopes are operating since 1996, and the last is being commissioned. These telescopes are part of the planned system of five placed at the corners of a square, 75 m long, and one in its center.

Strong arguments favour a system of Cherenkov telescopes since only the stereoscopic reconstruction [5,6] of Cherenkov images allows to suppress the background of hadronic showers and spurious local light sources. Thus it is expected that weak point sources and extended sources up to $\approx 1^\circ$ size can be detected. This task can be fullfilled only if the criteria for the optical performance of Cherenkov telescopes outlined in section 2 are met, which are different from optical telescopes used for astronomical observations.

The formalism of the raytracing program, which we developed for the calculations, is described in section 3. Raytracing calculations allow a realistic assessment of the image providing luminosity distributions, i.e. the spatial density of photons in the camera. This is important since the camera pixels have a coarse granularity in general. The calculated luminosity distributions allow to evaluate the fraction of light contained in a pixel and the leakage to adjacent ones.

Using the raytracing technique we have studied four reflector designs assuming similar diameter and focal length. Results are presented in section 4 for monolithic spherical and parabolic reflectors, the Davies-Cotton [7] design and finally the HEGRA design which employs 30 spherical mirrors with different focal lengths.

2. Optical Criteria for Cherenkov Telescopes

Photons of TeV energies as well as particles of the cosmic radiation are absorbed in the Earth's atmosphere. The absorption is accompagnied by a shower of charged ultrarelativistic particles, a so-called extended air shower (EAS) which in turn emits Cherenkov light. The Cherenkov light distribution is extended along the line of sight and has an intensity maximum at typically 10 km (asl) for 1 TeV primary energy. The mean angle of Cherenkov light with respect to the EAS axis is 1°. Approximately an area of 10^5 m^2 is illuminated by Cherenkov light on the ground, part of which is collected and registered by the Cherenkov telescopes.

Thus the optics of Cherenkov telecopes has to deal with a longitudinally extended object seen from the side i.e. emitting off-axis radiation. The field of view has to be larger than the lateral extent of the Cherenkov light distribution of 1° for

pointlike γ-sources and even larger for extended sources. If the telescope axis and the EAS axis coincide a circular extended light spot is obtained in the image plane of the telescope, otherwise the light distribution is noncircular. The directionality and the shape of the light spots are crucial for the distinction of γ-induced showers from cosmic ray induced showers. For a given field of view and granularity of the camera the optical layout for a Cherenkov telescope should map the Cherenkov light distribution and provide a *uniform, nondistorted* image of an off-axis line source.

Several authors [8–10] have investigated the necessary angular resolution i.e. the granularity of the camera and the field of view it should subtend. All analyses show that for realistic trigger conditions a granularity corresponding to a pixel size of $0.15^\circ - 0.25^\circ$ suffices for maximum detection rate and optimum distinction of γ-induced showers provided the field of view is $4^\circ - 5^\circ$ [10].

These simulations do *not* consider image distortions due to optical aberrations. The influence of realistic telescope imaging obtained from raytracing on the image parameters and consequently the telescope performance is presently investigated [11].

The HEGRA Cherenkov telescopes have a reflector dish with 30 mirrors and a camera with 271 pixels with an angular acceptance of 0.25° subtending a field of view of 4.75° [12]. In order to keep aberrations small the focal length f and the reflector diameter D should be chosen such that $f/D > 1$; for HEGRA the choice was $f \sim 5$ m and $D \sim 3.9$ m. The scale in the image plane is related to f and thus 0.25° corresponds to the flat to flat size of 21 mm of the hexagonal light concentrators attached to the photomultipliers (19 mm Ø) of the telescope camera [12]. The main aim for this investigation was to find an arrangement of 30 spherical mirrors with different focal lengths which has the best figure of merit. As a figure of merit of a Cherenkov telescope design we define the fraction of light emitted by a point source which is contained in one pixel for the full field of view.

We have also determined the isochronicity of the reflector designs. Since the duration of a Cherenkov 'flash' is only a few ns the optical system should not add more than ≈ 1 ns.

3. Evaluation of the Optical Performance

3.1. THE RAYTRACING FORMALISM

The basic geometry used in our raytracing program is shown in Figure 1. The components of a vector $\mathbf{r}$ from the apex of a spherical mirror to a point on its surface is given by

$$\mathbf{r} = R \cdot \Big(\sin(2u) \cdot \cos(t),\ \sin(2u) \cdot \sin(t),\ 2 \cdot \sin^2(u) \Big) \tag{1}$$

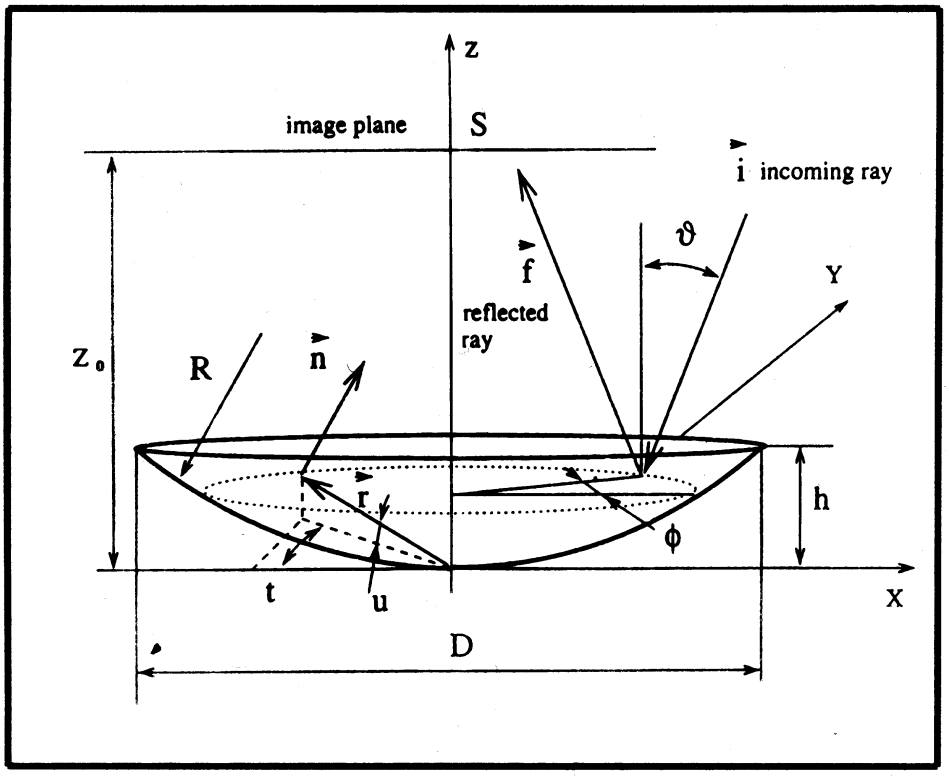

Figure 1. Sketch of the geometry of a spherical mirror.

with

$$0 \leq u \leq \arctan(2 \cdot h/D);\ 0 \leq t \leq 2\pi.$$

The parameter u is the angle between the (x, y)-plane and the radiusvector, t is the azimuthal angle with respect to the x-axis, and R denotes the radius of curvature of the mirror. The mirror diameter is given by D and h denotes the bulge of the mirror which is calculated from

$$h = R - \sqrt{R^2 - (D/2)^2}.$$

The components of the unit normal vector **n** at each surface point are then given by

$$\mathbf{n} = \Big(-\sin(2u) \cdot \cos(t),\ -\sin(2u) \cdot \sin(t),\ \cos(2u)\Big). \tag{2}$$

The direction cosines of an incoming ray **i** with angles (ϑ, ϕ) can be written as

$$\mathbf{i} = \Big(\sin(\vartheta) \cdot \cos(\phi),\ \sin(\vartheta) \cdot \sin(\phi),\ \cos(\vartheta)\Big). \tag{3}$$

The matrix $\mathbf{A}$ describing the reflection has the form

$$\mathbf{A} = \begin{pmatrix} 2n_x^2 - 1 & 2n_x n_y & 2n_x n_z \\ 2n_y n_x & 2n_y^2 - 1 & 2n_y n_z \\ 2n_z n_x & 2n_z n_y & 2n_z^2 - 1 \end{pmatrix}. \tag{4}$$

The direction cosines of the reflected ray $\mathbf{f} = (f_x, f_y, f_z)$ are calculated from

$$\mathbf{f}^T = \mathbf{A} \cdot \mathbf{i}^T \tag{5}$$

where $()^T$ stands for transposition.

The reflected ray $\mathbf{f}$ is intersected with the image plane at the distance z_0. The coordinates of the intersection point S are given by

$$\begin{aligned} s_x &= r_x + \lambda \cdot f_x \quad , \\ s_y &= r_y + \lambda \cdot f_y \quad , \\ s_z &= z_0 \end{aligned} \tag{6}$$

where $\lambda = (z_0 - r_z)/f_z$.

For a multi-mirror reflector consisting of n mirrors the position of the mth mirror ($m = 1...n$) on the dish is given by the coordinates (x_m, y_m, z_m) of its vertex and the direction of its normal by the angles (ϑ_m, ϕ_m), s. Figure 7. Then a radius vector $\mathbf{r}_m$ and its normal $\mathbf{n}_m$ are calculated for the mth mirror by the translation vector $\mathbf{p} = (x_m, y_m, z_m)$ and the rotation matrix

$$\mathbf{Q} = \begin{pmatrix} \cos(\vartheta_m) \cdot \cos(\phi_m) & -\sin(\phi_m) & \sin(\vartheta_m) \cdot \cos(\phi_m) \\ \cos(\vartheta_m) \cdot \sin(\phi_m) & \cos(\phi_m) & \sin(\vartheta_m) \cdot \sin(\phi_m) \\ -\sin(\vartheta_m) & 0 & \cos(\vartheta_m) \end{pmatrix} \tag{7}$$

yielding

$$\begin{aligned} (\mathbf{r}_m)^T &= \mathbf{Q} \cdot \mathbf{r}^T + \mathbf{p}^T \quad , \\ (\mathbf{n}_m)^T &= \mathbf{Q} \cdot \mathbf{n}^T \quad . \end{aligned} \tag{8}$$

The intersection point of the reflected ray with the image plane is then determined by Eq. 6.

The raytracing program has been written in IDL [13]. With the help of 'widget' routines consecutive tasks are defined, i.e. mirror setup, definition of rays, raytracing and various routines to evaluate the distribution of rays intersecting the image plane. Typically $3{\cdot}10^4$ rays are calculated which takes a few seconds of computer time.

In our program there are two options. In the first option only rays are calculated which are reflected from circles with specified coordinates u and $0 \leq t \leq 2\pi$ for each individual mirror. In the second option random values are chosen for the coordinates (u, t) of the mirror surface:

$$\begin{aligned} \cos(2u) &= 1 - \tfrac{h}{R} \cdot \xi \\ t &= 2\pi \cdot \eta \end{aligned} \tag{9}$$

TABLE I

The Seidel aberrations calculated from the formulae given in ref. [14,15] are compared to results from the raytracing program. The different values for the mirror diameter D, the image distance z_0 and the angle of incident rays ϑ are contained in the Table. For all cases the radius of curvature of the mirror is R = 9800 mm. Contributions from tangential and sagittal coma, C_t and C_s, respectively, were evaluated at different image distances z_0 according to ref. [15]. The coma aberrations are related by $C_t = 3 \cdot C_s$. Likewise the tangential and radial astigmatic aberrations, A_t and A_r were determined at the appropiate image distance according to ref. [15]. They are related to the so-called astigmatic size A_s by $A_r = 2 \cdot A_s$ and $A_t = 6 \cdot A_s$.

Type of aberration	predicted ref. [14] [mm]	predicted ref. [15] [mm]	ray tracing [mm]	D [mm]	z_0 [mm]	ϑ [°]
Spher. Aberr.	0.1406	0.1406	0.1408	600	4900	0
Coma C_s	0.1603	0.1603		600	4900	2
		0.1603	0.159	600	4897.70	2
		0.1606	0.161	600	4891.72	2
Astigm. A_s	0.2285	0.2267	0.2314	120	4918.72	5

where $\{\xi, \eta\}$ are randomly distributed in the interval [0,1]. This randomization has been chosen to cover homogeneously the available mirror surface.

3.2. Comparison of Seidel aberrations

The validity of our raytracing program has been proved by a comparison to the third order Seidel aberrations calculated with textbook formulae as e.g. given in ref. [14,15]. Here we summarize the results, which are presented in more detail in ref. [16].

The relevant optical aberrations are spherical aberration, coma, astigmatism and field distortion. The latter is not relevant for all designs discussed in this paper since it amounts to $\leq 1\%$ of the pixel size. The results calculated from textbook formulae are compared in Table I to those obtained with our raytracing program showing excellent agreement. The difference between the predicted and the raytracing result for the astigmatism A_s is due to contributions from the other aberrations.

In ref. [16] it is demonstrated that the textbook formulae are inadequate to reproduce the image size for large spherical mirrors ($f/D>1$) and far off-axis incoming rays. Furthermore even for paraxial rays reflected by a multimirror reflector the final image size is *not* a trivial addition of the Seidel aberrations proving the statement given in ref. [17]: *'... the general assumption that these errors are*

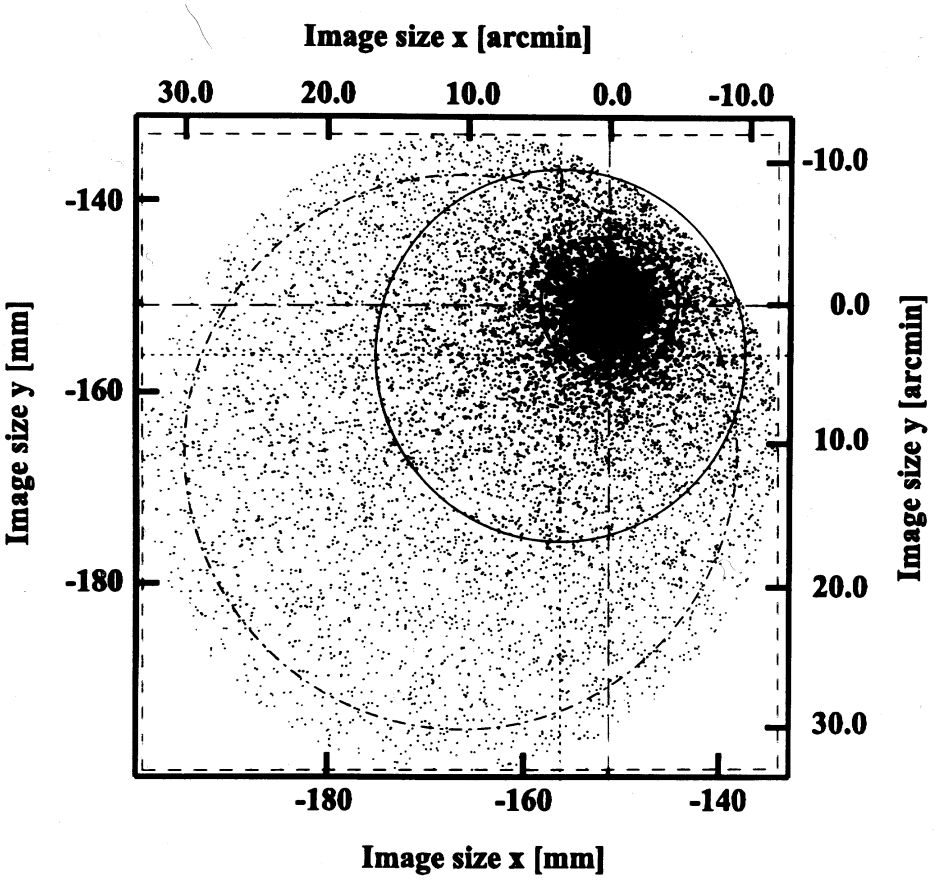

Figure 2. The light distribution in the image plane (z_0 = 4900 mm) of a monolithic spherical mirror with a diameter of D = 3446 mm for an incident angle of ϑ = 2.5° and ϕ = 45° is shown in fig. 2a. The geometric center **(a)** is indicated by the crossover of the long dashed lines, the center of gravity **(b)** of the dotted lines. The rectangle containing all rays is described by dashed lines. The solid circles around **(a)** and **(b)** define equivalent aperture radii $r_{eq}(\eta)$ for η = 50% and 80% light transmission, respectively. The dashed circle around the center of the rectangle **(c)** contains 95% of the light.

sufficient to decribe the quality of a lens (or mirrror) *with finite aperture and field of view ... is decidedly incorrect'.*

3.3. EVALUATION OF IMAGES

For rays parallel to the optical axis ($\vartheta = 0°$) of a symmetric reflector the intensity distribution in the image plane is also symmetric with respect to the optical axis. For larger angles of incidence this is not any more the case.

As an example Figure 2 shows the intensity distribution calculated for rays incoming at angles ϑ = 2.5° reflected in the image plane of a spherical mirror (s. Figure caption for details). Already for this case the analytical description of

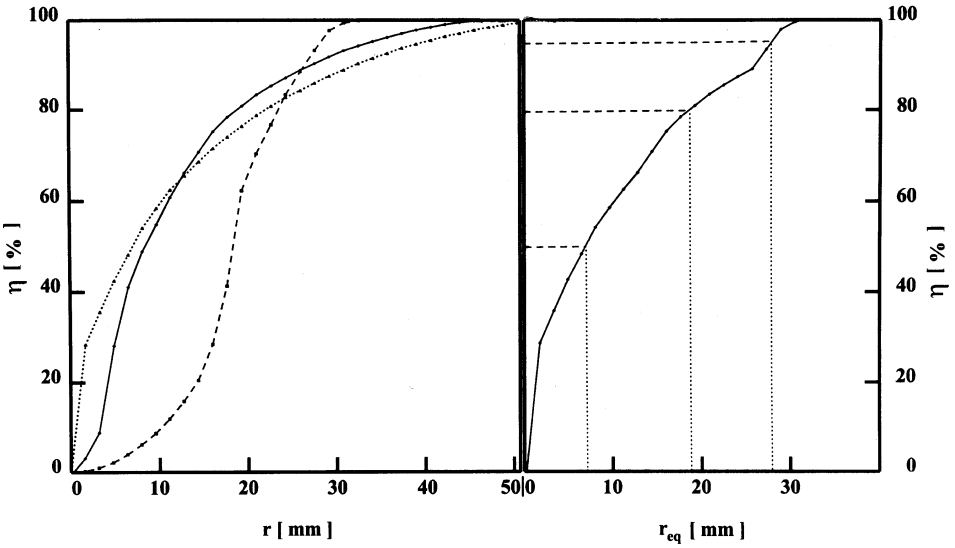

Figure 3. The integral light curves for the intensity distribution of fig. 2, i.e. η vs. $r_{eq}(\eta)$, are shown (fig. 3a, left) by the dotted, full and dashed lines assuming **(a)**,**(b)** and **(c)** as centers of the circular aperture. The curve composed from Figure 3a (left) for the evaluation of equivalent aperture radii r_{eq} is shown in Figure 3b (right).

contours of equal intensity becomes involved. It will be more complex if images have to be evaluated which are superimposed by several single mirrors. Another approach for earmarking the image quality is to evaluate the fraction of light which passes a collimator for which we have chosen a circular shape.

For an arbitrary intensity distribution the center of a circular collimator of given radius should be determined which passes the maximum light. Then the radius is varied and the search for maximum light transmission is repeated. Finally for the specific intensity distribution a relation is obtained between collimator radius and maximum transmission.

Since for most cases investigated here the maximum intensity is close to the optical center **(a)** or the center of gravity of the intensity **(b)** we have chosen those as centers of circular collimators of different radii r. The transmitted fraction of light η vs. r is plotted in Figure 3aa for the intensity distribution shown in Figure 2. Both curves show that for $\eta \approx 100\%$ the calculated radius exceeds the maximum size of the rectangle containing all rays by a factor of up to 2. The size of the tail of the intensity distribution is overestimated. Therefore we have chosen the center of the rectangle **(c)** for a similar evaluation of η vs. r – as also shown in Figure 3a. This describes the tail correctly, but overestimates the radii for small values of η. We have evaluated the light transmission η using the three prescriptions and have derived a composed curve denoted as 'integral light curve' where for a given light transmission η the minimum radii are taken which are denoted by r_{eq}, see

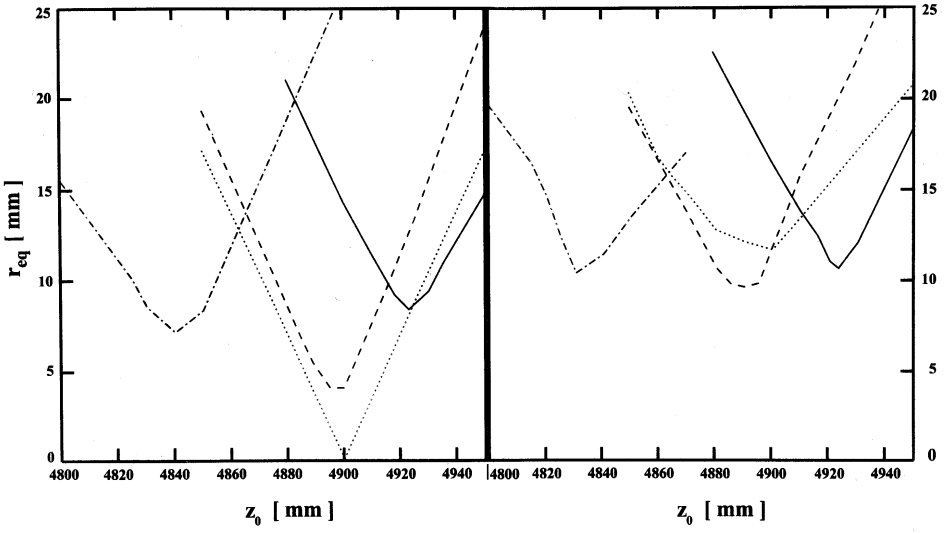

Figure 4. Dependence of the equivalent aperture radius $r_{eq}(95)$ on the image distance z_0 for incident angles of $\vartheta = 0°$ (Figure 4a, left) and 2.5° (Figure 4b, right). The curves correspond to the monolithic spherical (dot-dashed) and parabolic (dotted) mirrors, the Davies-Cotton layout (dashed) and the HEGRA design (full).

Figure 3b. In the following we mostly use $r_{eq}(50)$ and $r_{eq}(95)$ corresponding to the collimator radius for 50% and 95% light transmission, respectively.

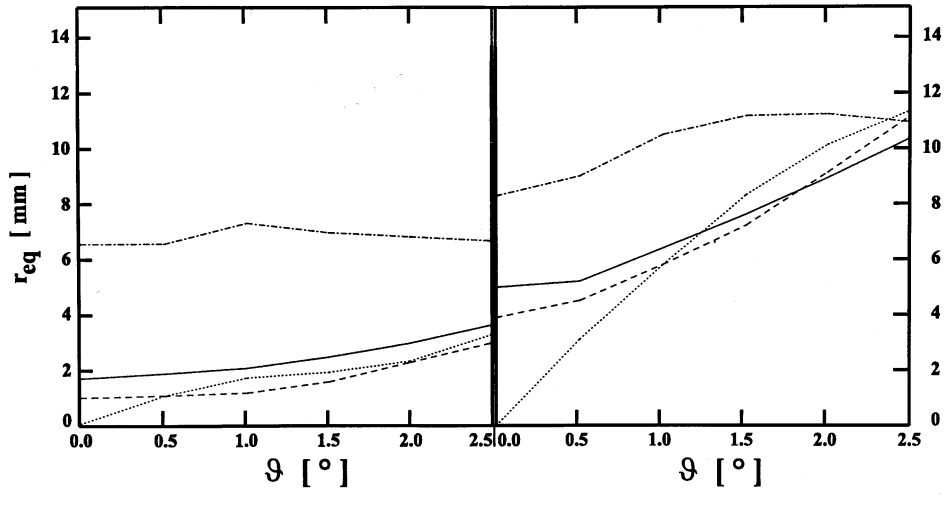

Figure 5. The equivalent aperture radius $r_{eq}(50)$ (Figure 5a, left) and $r_{eq}(95)$ (Figure 5b, right) of the four reflector designs (s. caption of Figure 4) are shown for the full field of view i.e. $0° \leq \vartheta \leq 2.5°$.

4. Reflector Design for Cherenkov Telescopes

Existing and planned Cherenkov telescopes employ either parabolic [18,19] or spherical reflectors [4, 20-22] and consist of an arrangement of individual mirrors. Focal length and reflector diameter vary substantially. Among the further differences are e.g. the tessalated structure – as for the Whipple reflectors [20] – compared to the hexagonal package of circular mirrors as for the HEGRA Cherenkov telescopes [4].

We have investigated in a first step monolithic reflectors with *ideal* spherical and parabolic surfaces. Then the optics of the commonly used Davies-Cotton design [7] has been investigated for an arrangement of 30 identical spherical mirrors, which have a diameter of 600 mm and finally the HEGRA design using 30 mirrors with different sphericity.

The diameter of the HEGRA reflector defined as the maximum edge to edge distance between opposite mirrors determined by the hexagonal package of the 30 mirrors is D_0 = 3881 mm. The reflecting area thus is A = 8.48 m^2. For a comparison of the optical performance of the multi-mirror designs we have investigated monolithic reflector designs with the same f-number of $\approx f/1.4$.

4.1. MONOLITHIC REFLECTORS

4.1.1. *The spherical mirror*

Raytracing calculations were performed for a spherical mirror with a diameter of D_m = 3446 mm and a radius of curvature of 9800 mm. For each set of angles (ϑ, ϕ) of rays with ϕ = 45° and ϑ in the range of 0° $\leq \vartheta \leq$2.5° rays have been traced to the image plane placed at z_0 = 4900 mm. Fig. 2 shows the light distribution for ϑ = 2.5° from which the integral light curve (Figure 3b) and the equivalent radii, $r_{eq}(50)$ and $r_{eq}(95)$, have been evaluated. The results are $r_{eq}(95)$ = 28 mm corresponding to $\approx$ 20 arcmin for ϑ = 2.5° and $r_{eq}(95)$ = 25 mm ($\approx$ 17 arcmin) for ϑ = 0°.

We have investigated the effect of a shift of the image plane distance z_0 on the image size as shown in Figure 4 where $r_{eq}(95)$ is plotted versus z_0 for incident angles of ϑ = 0° and 2.5°. A minimum of $r_{eq}(95)$ is obtained for ϑ = 2.5° at z_0 = 4835 mm. A similar result, z_0 = 4841 mm, is calculated according to ref. [15] where an analytical expression for the minimum spot size of a spherical reflector has been derived. Fig. 5 shows the variation of $r_{eq}(50)$ and $r_{eq}(95)$ for the full field of view (0° $\leq \vartheta \leq$ 2.5°), where z_0 corresponds to the image distance for minimum spot size.

4.1.2. *The parabolic reflector*

For a parabolic mirror eqs. (1-3) in section 3 have to be modified. The components of the vector $\mathbf{r}_p$ to a point on the parabolic surface is given by

$$\mathbf{r}_p = 4f \cdot \Big(\tan(u) \cdot \cos(t),\ \tan(u) \cdot \sin(t),\ \tan^2(u)\Big) \tag{10}$$

with

$$u = arctan\Big(\frac{1}{2}\sqrt{(1+(w^{3/2}-1)\cdot\xi)^{2/3}-1}\Big)$$

where

$$w = 1 + (\frac{D}{4\cdot f})^2.$$

Here ξ is randomly chosen in the interval [0,1] and $0 \leq t \leq 2\pi$. The components of the unit normal vector $\mathbf{n}_p$ at any surface point are then given by

$$\mathbf{n}_p = c\cdot\Big(-2\cdot\tan(u)\cdot\cos(t),\ -2\cdot\tan(u)\cdot\sin(t),\ 1\Big) \tag{11}$$

with

$c^{-1} = \sqrt{1+4\cdot\tan^2(u)}$.

For axial incidence ($\vartheta = 0°$) the focussing is perfect i.e. the spot size is zero. The light distribution for nonaxial incidence shows the typical v-shape (s. Figure 6). The equivalent aperture radius $r_{eq}(95)$ grows almost linearly with ϑ to $r_{eq}(95)$ = 13 mm for ϑ = 2.5°.

Fig. 4 shows the dependence of $r_{eq}(95)$ on the image distance z_0 for ϑ = 0° and 2.5°. In Figure 5 the variation of $r_{eq}(50)$ and $r_{eq}(95)$ is displayed for the full field of view.

4.2. Reflector designs with segmented mirrors

4.2.1. *Geometry of the reflector*

In this section a specific arrangement of spherical mirrors on the reflector dish is discussed, which is realized in the HEGRA Cherenkov telescopes.

The left part of Figure 7 shows the projection of the 30 mirrors. In order to obtain tight packaging the mirrors were centered into a contiguous hexagonal pattern. For technical reasons the cell width was chosen to be 620 mm for the mirrors with a diameter of 600 mm. Thus 6 mirrors each lie on two circles with radii R_1 = 620 mm and $R_2 = \sqrt{3}\cdot R_1$ = 1073.9 mm, respectively, whereas 12 mirrors each are centered on the two outer circles with radii $R_3 = 2\cdot R_1$ = 1240 mm and $R_4 = \sqrt{7}\cdot R_1$ = 1640.4 mm, respectively.

In this hexagonal pattern the (x_m, y_m) coordinates and hence the azimuth angle ϕ_m of the mth mirror are fixed. The z_m mirror coordinates are calculated with an assumed radius of curvature ρ_m of the mth mirror,

$$z_m = \rho_m - \sqrt{\rho_m^2 - x_m^2 - y_m^2}. \tag{12}$$

The mirror tilt angle θ_m is defined by the intersection of the normal vector $\mathbf{n}$ and the z-axis of the reflector. For the mirrors lying on a circle with radius R_i it is given by:

$$\theta_m = \arctan\Big(\frac{R_i}{\rho_m - z_m}\Big) \tag{13}$$

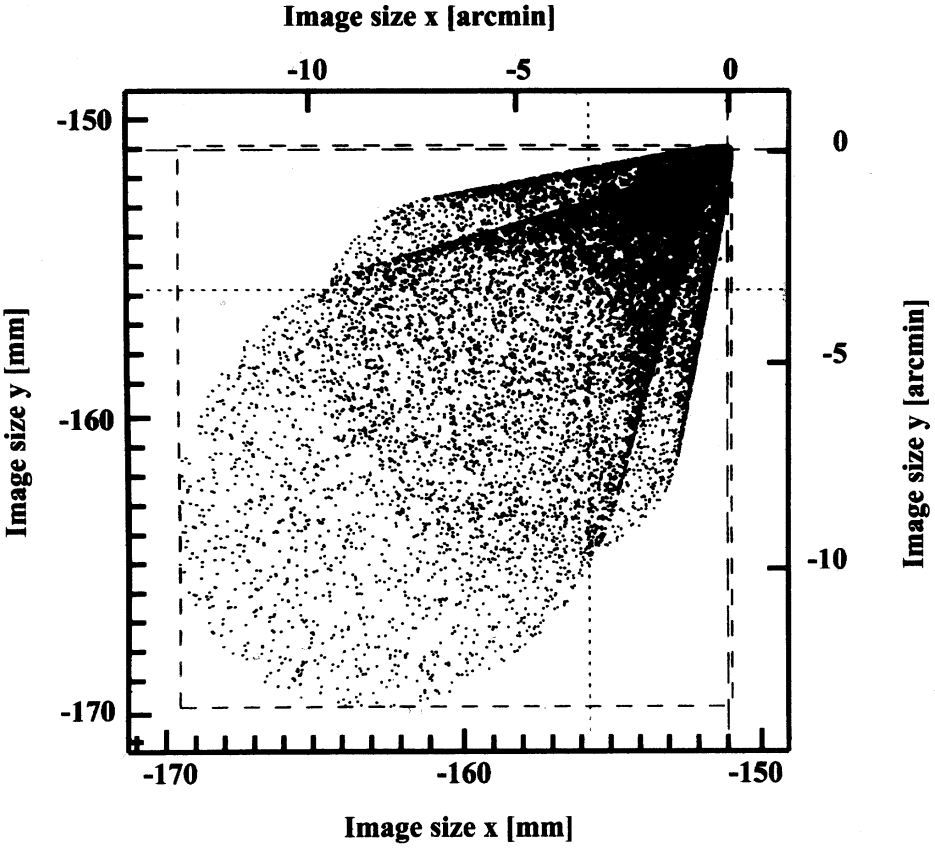

Figure 6. The light distribution of a parabolic mirror is evaluated at an image distance z_0 = 4900 mm for an incident angle of ϑ = 2.5° and ϕ = 45°.

where

$$R_i = \sqrt{x_m^2 + y_m^2}, \quad i = 1...4.$$

4.2.2. *The Davies-Cotton design*

In an effort to find an economic realization for a solar furnace Davies and Cotton [7] have suggested a square concentrator dish (8.5×8.5 m^2) with a focal length of f = 10.92 m which contains 180 spherical mirrors. The primary aim was to concentrate the light of the Sun by a factor >5000 homogeneously into a spot ≈ 100 mm in diameter. It is worthwile to note that this specification implies a rather small field of view since the diameter of the Sun is ∼ 0.5°. Davies and Cotton suggested to employ spherical mirrors with identical focal length. They are mounted on a dish, which has a radius of curvature of $R_d = f$ (Figure 7, left). The image plane is defined at a distance $z_0 = f$ and the mirror tilt angles θ_m were

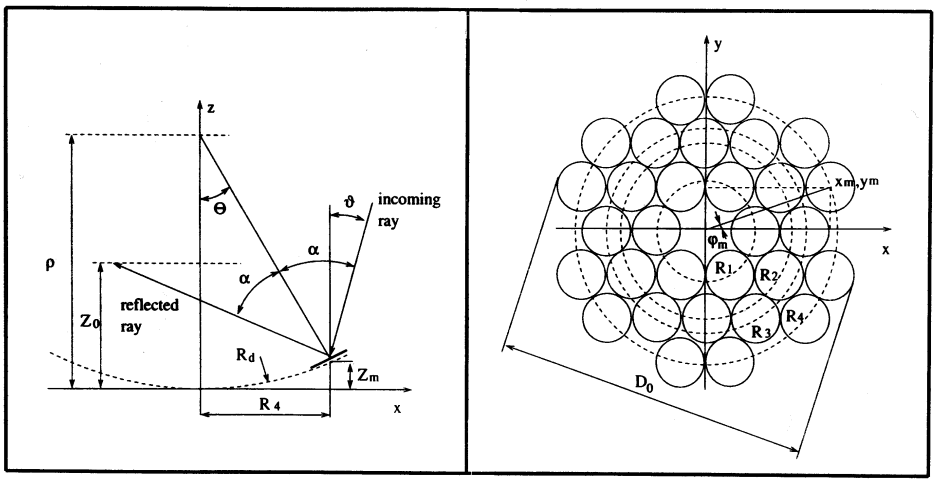

Figure 7. Geometry of the segmented reflector containing 30 mirrors.

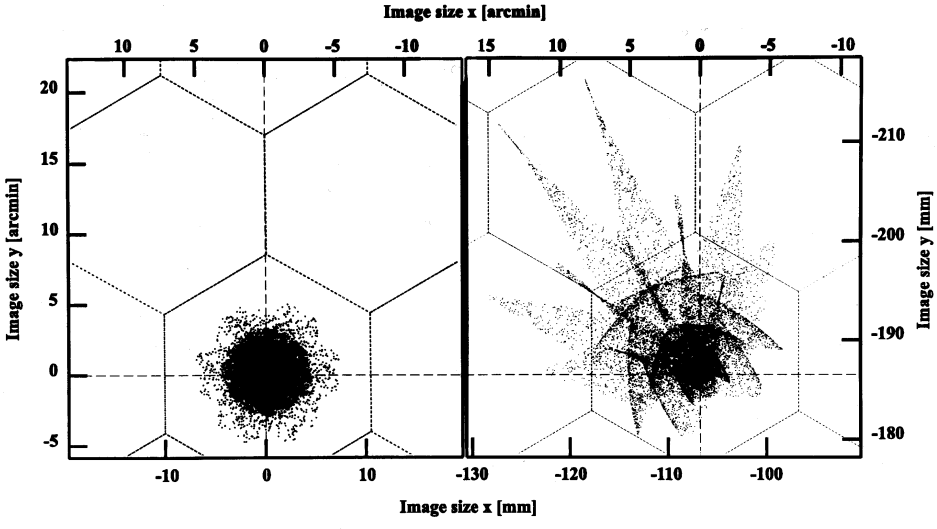

Figure 8. The light distributions of the Davies-Cotton design evaluated at an image distance z_0 = 4900 mm are shown for rays incident at ϑ = 0° (Figure 8a, left) and 2.5° (Figure 8b, right). The dotted hexagons represent the pixels of the HEGRA camera.

determined according to Eq. 13. The radius of curvature is assumed to be constant, $\rho_m = 2 \cdot f$.

We have studied a reflector design of 30 identical spherical mirrors with focal lengths of f = 4900 mm in the geometry outlined in section 4.2.1 and shown in Figure 7. Intensity distributions for ϑ = 0° and 2.5° are shown in Figure 8 for an image distance of z_0 = 4900 mm. The integral light curves extracted for ϑ in the

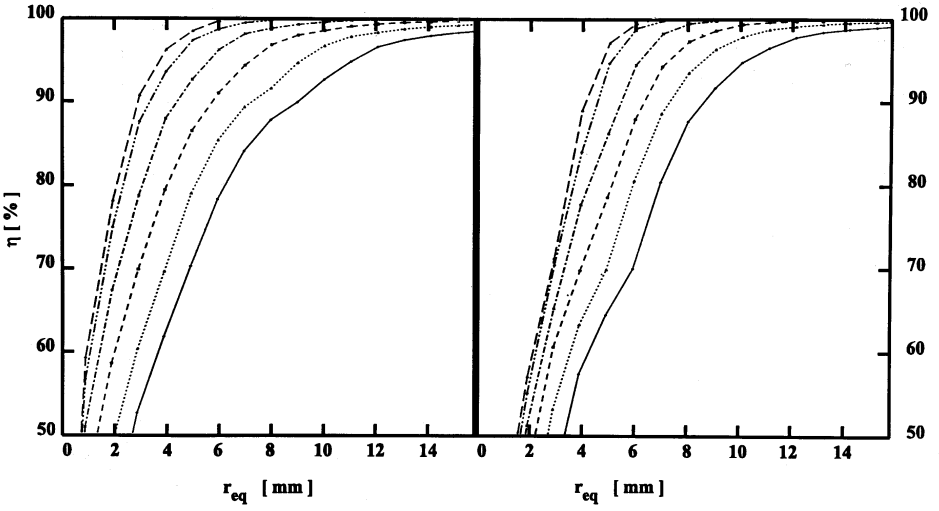

Figure 9. The integral light curves characterizing the Davies-Cotton design for $0° \leq \vartheta \leq 2.5°$, in steps of 0.5°, at an image distance z_0 = 4900 mm (Figure 9a, left) and the HEGRA layout (Figure 9b, right) at z_0 = 4923 mm with $\delta\theta$ = + 0.9 arcmin. For ϑ = 2.5° (full line) we find $r_{eq}(95)$ = 10.9 mm and $r_{eq}(95)$ = 10.0 mm for the Davies-Cotton and HEGRA design, respectively.

interval [0°, 2.5°] in Figure 9a indicate that 95% of the light is contained in a pixel with a diameter of 0.25° corresponding to $r_{eq}(95)$ = 10.9 mm even for ϑ = 2.5°.

The dependence of $r_{eq}(95)$ on the image plane distance z_0 for $\vartheta = 0°$ and 2.5° is shown in Figure 4. A 15% change of $r_{eq}(95)$ in the case of $\vartheta = 2.5°$ is found for $\delta z_0 = \pm$ 10 mm. In Figure 5 the variation of $r_{eq}(50)$ and $r_{eq}(95)$ is displayed for the full field of view for z_0 = 4900 mm.

Following a suggestion by Davies and Cotton [7] and in ref. [23] that the image is improved by 'advancing' peripheral mirrors 'in the direction of the incoming beam' we have varied the $z_m^{i=4}$-coordinate of the 12 mirrors on the fourth ring up to 50 mm from its original position.

Indeed for a shift of $\delta z^{i=4}$ = 15 mm the equivalent radius $r_{eq}(95)$ was reduced by 15% for ϑ = 2.5°. At the same time however the quantity $r_{eq}(50)$ is increased by 20%. It should be mentioned that these results depend critically on the specified light transmission η, e.g. for η = 70% the equivalent radii $r_{eq}(70)$ are affected negligibly ($\leq$ 1mm) for ϑ = 0° and 2.5° by such a shift.

The greatest sensitivity was found for a variation of the mirror tilt angle θ_m being most pronounced for the peripheral mirrors. Therefore we have applied a variation $\delta\theta$ which increases linearly from the innermost mirrors to the outer ones – all mirrors in the ith ring are treated alike:

$$\theta_m^i = \theta_m^{i=2} + (i-2) \cdot \delta\theta, \quad i = 1...4 \tag{14}$$

where the tilt angle $\theta_m^{i=2}$ is calculated from Eq. 13.

For rays incident at an angle of ϑ = 2.5° the equivalent aperture radii $r_{eq}(50)$ and $r_{eq}(95)$ were found to depend quadratically on a tilt angle variation $\delta\theta$ within a range of $\pm$ 1 arcmin, with a minimum at $\delta\theta$ = - 0.3 arcmin, i.e. close to the unperturbed value. Both equivalent radii increase by $\approx$ 20% for a change of $\delta\theta$ = $\pm$ 1 arcmin.

4.2.3. *The HEGRA reflector design*

As in any fabrication process the actual sphericity scatters around a mean. Since costs rise rapidly with a reduction of the tolerances, the main aim of this study was to search for and investigate the optical performance of arrangements, which employ mirrors of different sphericity and meet the design criteria specified in section 2.

It turns out that these criteria can be met by a variety of designs using the Davies-Cotton prescription as the 'design of departure'. Consequently the sphericity tolerances have been alleveated.

The Optics Department of the Yerevan Physics Institute provided the mirrors for the HEGRA Cherenkov telescopes which were ground from glass discs [4]. The distribution of focal lengths extends over a wide range, $4810 \leq f$ [mm] $\leq$ 4970 with about 60% of the mirrors having a focal length between 4890 and 4910 mm.

As one specific arrangement of the 30 mirrors all mirrors in a given ring are chosen to have identical focal length. The second ring (R_2 = 1073.9 mm) was treated as the reference ring containing mirrors with $f = f_0$. The focal length f^i of the mirrors in the ith ring was assumed to differ from f_0 by δf according to

$$f^i = f_0 + (i - 2) \cdot \delta f, \quad i = 1...4. \tag{15}$$

In our design we choose f_0 = 4900 mm and δf = 20 mm.

The coordinates z_m of the mirrors were determined from Eq. 12. The mirror tilt angles θ_m^i were calculated from Eq. 13. The dependence of r_{eq} (95) on the image plane distance z_0 is displayed in Figure 4 for ϑ = 0° and 2.5°. It is similar to that of the Davies-Cotton design, however the minimum value of $r_{eq}(95)$ is found at z_0 = 4923 mm. In Figure 5 the variation of $r_{eq}(50)$ and $r_{eq}(95)$ is displayed for the full field of view for z_0 = 4923 mm.

The sensitivity of $r_{eq}(95)$ on a variation of the mirror tilt angle $\delta\theta$ was found to be similar to the Davies-Cotton design with a pronounced minimum for $\delta\theta$ = + 0.9 arcmin. A departure from this value by $\delta\theta = \pm$ 1.2 arcmin increases $r_{eq}(95)$ by 25%. The effect on $r_{eq}(50)$ is less. These results are obtained at the edge of the field of view (ϑ = 2.5°) and are less for smaller values of ϑ.

For the following investigations we used z_0 = 4923 mm and $\delta\theta$ = + 0.9 arcmin. The integral light curves are shown in Figure 9b. In contrast to the Davies-Cotton design an advance of the mirrors of the 4th ring in the range of $\delta z_m = \pm$ 20 mm does *not* decrease $r_{eq}(95)$.

TABLE II

Fraction of light η contained in a hexagonal camera pixel for the HEGRA design for different angles of incidence ϑ

ϑ	0	0.5	1	1.5	2	2.5	[°]
η	100	100	100	99.9	98.2	93.5	[%]

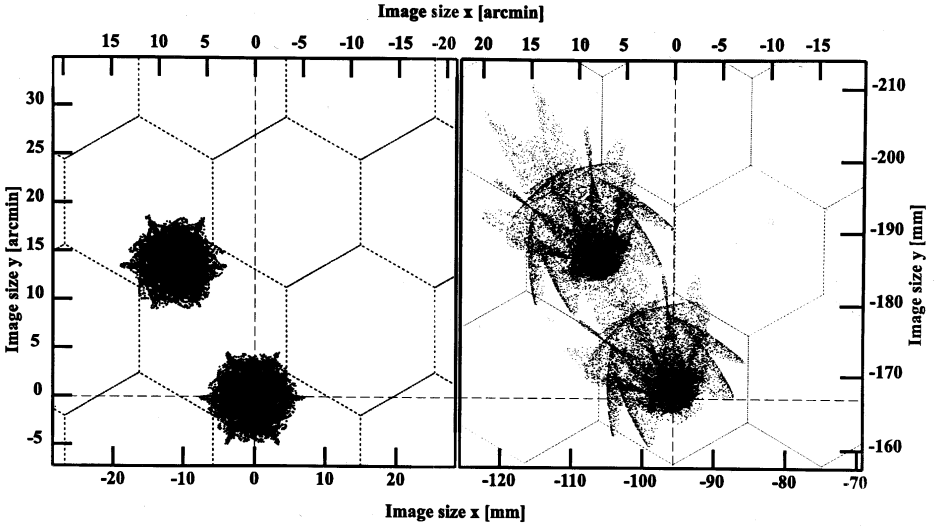

Figure 10. Light distribution of two sources separated by 0.25° for incident angles of ϑ = 0°, 0.25° (Figure 10a, left) and ϑ = 2.25°, 2.5° (Figure 10b, right) for the HEGRA design (z_0 = 4923 mm, $\delta\theta$ = + 0.9 arcmin).

For the HEGRA design the quality of containment of photons in a hexagonal pixel was investigated. To this purpose two light sources have been traced which are separated by $\delta\vartheta$ = 0.25°. The resulting scatter plots evaluated at an image distance of z_0 = 4923 mm are shown in Figure 10a (ϑ = 0°) and in Figure 10b (ϑ = 2.5°). The overlaid hexagonal grid represents the boundaries of the light funnels feeding the photomultipliers. The number of photons which leak into neighbouring pixels has been evaluated. In Table II the fraction of photons η contained in one pixel is listed for rays incident at angles ϑ between 0° and 2.5°.

5. Summary of Results

Our investigations of designs for imaging Cherenkov telescopes include two monolithic mirrors and two layouts for multi-mirror arrangements of 30 spherical mir-

rors. For all designs the f-number, $f/1.4$, is the same. For the four studied designs the equivalent radii $r_{eq}(50)$ and $r_{eq}(95)$ are shown for angles of incidence $\vartheta \leq 2.5°$, i.e. the full field of view in Figure 5. The image distance z_0 was chosen such that $r_{eq}(95)$ is minimum. It is seen that a pixel with a diameter of 0.25° corresponding to a radius of 7.5 arcmin contains 93% of the Cherenkov photons even for $\vartheta = 2.5°$. The HEGRA design has a performance similar to the Davies-Cotton layout.

The investigated reflector layouts differ in their sensitivity to variations of the image distance z_0 as shown in Figure 4. For the HEGRA design the 'advance of the outer mirrors' from the spherical dish has a small effect on the spot size. The most critical parameter of the multimirror designs is the orientation angle of the mirrors.

Isochronicity was mentioned in section 2 as an important specification. To that purpose the difference in time of the maximum and minimum trajectory has been determined for the four reflector designs. For the monolithic (spherical and parabolic) mirrors we obtained $\delta t_i = 0.5$ ns, for the multi-mirror (Davies-Cotton and HEGRA) designs $\delta t_i = 1.2$ ns. For a small field of view ($\vartheta \approx 0$) the parabolic mirror has perfect isochronicity and the spherical mirror a small deviation from isochronicity ($\delta t_i = 0.03$ ns), whereas the multi-mirror designs already have $\delta t_i = 0.8$ ns.

The aim of the present study was to search for a suitable design for the HEGRA Cherenkov telescopes employing 30 mirrors with sphericities differing by $\approx 1\%$. The overall optical performance according to our investigations does not depend on the exact focal length of an individual mirror. The chosen staggering of focal lengths of 20 mm for mirrors in adjacent rings – the quantity δf in Eq. 15 – constitutes a 'shallow optimum'. In fact we varied δf by $\pm$ 40 mm and find that after a readjustment of the image distance z_0 the equivalent radii for 95% light transmission increase by 10% for a 10 mm increase in δf. These values refer to an angle of incidence of $\vartheta = 2.5°$ and are smaller for a smaller field of view. The optical performance of the Davies-Cotton and the HEGRA design specified in terms of equivalent aperture radii r_{eq} differ depending on the choice of the value for the light transmission η: For $\eta \geq 90\%$ the HEGRA layout provides a smaller equivalent radius, for $\eta \leq 90\%$ this holds true for the Davies-Cotton design.

The HEGRA design discussed in this paper does not constitute an optimum layout for Cherenkov telescopes. It rather serves as a guideline to construct and evaluate adequate designs with similar f-number employing mirrors with different focal length.

Acknowledgements

Two of the authors (A. A. and R. K.) extend their gratitude to the Max-Planck-Institut für Kernphysik, Heidelberg for its hospitality encouraging this study. In particular we want to thank Prof. W. Hofmann, Prof. H. Völk, Dr. F. A. Aharonian

and Dr. R. Mirzoyan for helpful discussions. Finally we appreciate the comments of many colleagues from the HEGRA collaboration.

References

Thompson, D. J. *et al*.: 1995, *Ap. J. Supp. Vol.* **101**, 259.
References in 'Towards a Major Cerenkov Detector III' (ed. T. Kifune), Tokyo 1994.
Aharonian, F. A. *et al*.: 1989, Proposal for Imaging Air Cherenkev Telescopes in the HEGRA Particle Array, Kiel (unpublished).
Mirzoyan, R. *et al*.: 1994, *Nucl. Instr. Meth.* **A 351**, 13.
Turver, K. E.: 1996, in H. J. Völk and F. A. Aharonian (eds.), 'Proceedings of the Heidelberg Workshop on TeV Gamma-Ray Astrophysics', *Space Sc. Rev. Vol.* **75**, Nos. 1–2.
Aharonian, F. A.: 1994, in T. Kifune (ed.), 'Towards a Major Atmospheric Cerenkov Detector III' Tokyo.
Davies, J. M. and Cotton, E. S.: 1957, *J. Solar En.* **1**, 16.
Aharonian F. A. *et al*.: 1995, *J. Phys. G: Nucl. Part. Phys.* **21**, 985.
Zyskin, Y. *et al*.: 1994, *J. Phys. G.: Nucl. Part. Phys.* **20**, 1851.
Fomin, V. P. *et al*.: 1995, *Astrop. Phys.* **4**, 113.
Akhperjanian, A.: priv. communication.
Panter, M.: 1995, Proc. 24th Int. Cosmic Ray Conf., Rome, 958.
Interactive Data Language Systems Inc., Boulder (1993).
Michelson, I. I.: 1976, Optischeskie Teleskopie, Isv. Acad. Nauka, Moskwa.
Smith, W. J.: 1966, Modern Optical Engineering, McGraw-Hill Inc., New York.
Akhperjanian, A. *et al*.: 1995, 'The Optical Layout of the HEGRA Cherenkov Telescopes', Report MPI-H-V46-1995, Heidelberg, (unpublished).
Herzberger, M.: 1964, in R. K. Luneburg (ed.), 'Mathematical Theory of Optics' Univ. of Calif. Press, Berkeley and Los Angeles, p. 440.
Goret, P. *et al*.: 1993, *Astron. Astrophys* **270**, 401.
Hara, T. *et al*.: 1993, *Nucl. Instr. Meth.* **A 332**, 300.
Lewis, D. A.: 1990, *Exp. Astron.* **1**, 213.
Degrange, B. *et al*.: 1993, 'Cherenkov Array at Themis (CAT)', project report, Palaiseau, (unpublished).
Baillon, P. *et al*.: 193, *Astrop. Phys.* **1**, 341.
Mirzoyan, R., Fomin, V. P. and A. Stepanian: 1996, *Nucl. Instr. Meth.* **A 373**, 153.